SWIFT XRT Point Spread Function measured at the Panter end-to-end tests *

A. Moretti[a], S. Campana[a], G. Tagliaferri[a], A.F. Abbey[c], R.M. Ambrosi[c], L. Angelini[g h], A. Beardmore[c], H.W. Bräuninger[e], W. Burkert[e], D.N. Burrows[b], M. Capalbi[d], G. Chincarini[a], O. Citterio[a], G. Cusumano[f], M.J. Freyberg[e], P. Giommi[d], G.D. Hartner[e], J.E. Hill[b], K. Mori[b], D. Morris[b], K. Mukerjee[c], J.A. Nousek[b], J. Osborne[c], A.D.T. Short[c], F. Tamburelli[d], D.J. Watson[c], A. Wells[c]

[a] INAF Osservatorio Astronomico di Brera, Italy
[b] Pennsylvania State University, USA
[c] University of Leicester, UK
[d] Agenzia Spaziale Italiana, Italy
[e] Max-Planck-Institut für Extraterrestrische Physik, Germany
[f] CNR Istituto di Fisica Cosmica ed Applicazioni dell' Informatica, Italy
[g] LHEA, GSFC/NASA
[h] USRA

ABSTRACT

The *SWIFT* X–ray Telescope (XRT) is designed to make astrometric, spectroscopic and photometric observations of the X–ray emission from Gamma–ray bursts and their afterglows, in the energy band 0.2-10 keV. Here we report the results of the analysis of *SWIFT* XRT Point Spread Function (PSF) as measured during the end-to-end calibration campaign at the Panter X–Ray beam line facility. The analysis comprises the study of the PSF both on–axis and off–axis. We compare the laboratory results with the expectations from the ray–tracing software and from the mirror module tested as a single unit. We show that the measured HEW meets the mission scientific requirements. On the basis of the calibration data we build an analytical model which is able to reproduce the PSF as a function of the energy and the position within the detector.

Keywords: Swift, XRT, PSF

1. INTRODUCTION

The XRT[1] is a sensitive, autonomous X-ray CCD imaging spectrometer designed to measure the flux, spectrum, and light curve of GRBs and afterglow over a wide flux range covering more than seven orders of magnitude in flux. XRT utilizes the third flight mirror module (FM3) developed for the JET–X program[2]: it consists of 12 nested, confocal and coaxial mirror shells having a Wolter I configuration. The mirror diameters range from 191 mm to 300 mm, the nominal focal length is 3500 mm, the total field of view is about 40 arcminutes (at

Copyright 2004 Society of Photo-Optical Instrumentatio Engineers This paper will be published in *Proc. SPIE*, Vol. 5165, and is made available as an electronic preprint with permission of SPIE. One print or electronic copy may be made for personal use only. Systemetic or multiple reproduction, distribution to multiple locations via electronic or other means, duplications of any material in this paper for a fee or for commercial purposes, or modification of the paper are prohibited.

Send correspondence to moretti@merate.mi.astro.it

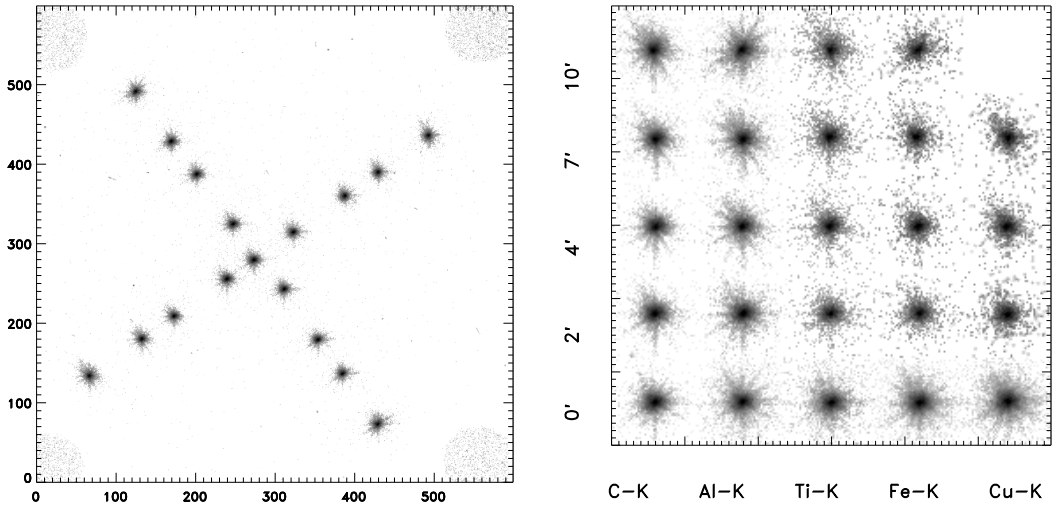

Figure 1. The left panel shows the different positions used to study the PSF on- and off–axis in the case of the Al-K: it is produced summing different images taken at different times. The right panel shows the mosaic of different images and represents the grid of the energies and positions we used in our study.

50% vignetting level) and the effective area at 1.5 keV is $\sim$ 165 cm^2. The XRT imaging array is a MAT-22 CCD consisting of 600 x 600 pixels, each 40μm $\times$40μm with a nominal plate scale of 2.36 arcseconds per pixel, which makes the effective field of view of the system $\sim$ 24 arcmin.[1] The instrument response of 1 counts sec^{-1} corresponds to a source flux of $\sim$ 1 mCrab. The JET–X flight modules FM1 and FM2 have already been tested during the JET–X end-to-end calibration[3] in March/April 1997 at the Panter laboratory of the Max-Plank-Institut für Extraterrestrische Physik. The spare FM3 mirror module has been calibrated as a single unit in July 2000[4] at the same facility. A ray–tracing code has been developed to evaluate the response of the telescope for the purpose of the JET–X mission. This software takes into account the nominal geometry of the telescope and the main physical effects of the focusing process: gold reflectivity and scattering microroughness.[5]

The Panter end-to-end calibration campaign of the *SWIFT* XRT has been carried out in the period September 23rd - October 4th 2002. In particular the PSF calibration aimed to confirm that the mounting of the mirror inside XRT did not introduce distortions.

Table 1. The values of the 5 calibration energies used for PSF calibration.

source	C-K	Al-K	Ti-K	Fe-K	Cu-K
energy [keV]	0.28	1.49	4.51	6.40	8.05

2. THE DATA

PSF calibration data have been collected at five energies (Tab.1) both on–axis and at four off–axis angles in two perpendicular directions (Fig.1). The left panel of this figure shows how the sources have been moved along a grid of position within the detector and the right panel represents the grid of energies and positions we used in our analysis. The data for PSF calibration have been taken in imaging mode. This operational mode is suited to determine the position of the GRB immediately after the spacecraft has slewed and settled on the target: the charge produced by the X–ray events is read directly without the event reconstruction, keeping the spatial information and losing most of the energetic information of the accumulated events. This allows us to observe bright sources without any distortion of their surface brightness profile in a very large range of fluxes and therefore it is the fastest way to accumulate data keeping the spatial information (however it does not allow to collect meaningful spectra). In an imaging frame the value registered in each pixel is the amount of charge accumulated in the frame interval and can be all the charge of one event, or a fraction of a splitted event or the sum of different events: this implies that the calculation of the number of the observed events without any event reconstruction procedure is not a trivial task. The histogram of the pixel values of the images is characterized by the peak of the single pixel events which contains all the charge of one event and has a typical value for each monochromatic energy (Fig.2). Dividing the value of the accumulated charge in each pixel by the typical value of the single event gives a good approximation of the number of the events accumulated in the image of a source. In imaging mode the data are reliable without any PSF distortion up to $\sim$ 30,000 counts sec^{-1}. Beyond this point the out-of-time events effect cannot be ignored: this effect can slightly modify the PSF profile (it does not affect the calculation of the centroid). For the PSF calibration we selected the observations with more than 1,000 total counts in the image, taken with a count rate lower than 10,000 counts sec^{-1} at the CCD: in Fig 3 we report for each bin in the Energy-Position plane the numbers of reliable observations we used for our analysis.

3. THE POINT SPREAD FUNCTION

The analysis of the XRT PSF has been performed assuming a radial dependence of the PSF. The radial profile PSF(r) has been built counting the charge contained within annuli of different width. In the inner PSF regions, close to the centroid, where the slope of the profile is very steep we sample the PSF with annuli of 1/5 pixel of width. In the external part of the PSF, where the number of counts is low we sample the profile on scale of 10 or 20 pixels. For each choice of monochromatic energy and position the PSF profile can be well fitted by a model composed by a Gaussian function that takes into account the very central part of the profile and a King function which describes the external faint wings (Fig. 4):

$$PSF(r) = We^{-\frac{r^2}{2\sigma^2}} + (1-W)(1+(\frac{r}{r_c})^2)^{-\beta}). \qquad (1)$$

The model has 4 free parameters (plus the total normalization) W, σ, r_c, β which are functions of the energy E and position θ: W=W(E,θ), $\sigma = \sigma$(E,θ), $r_c = r_c$(E,θ), $\beta = \beta$(E,θ). Typical values of the parameters for the on–axis PSF at different energies are reported in Tab. 2. One of the main advantages of this function is that it is analytically integrable in rdr and therefore the integral profile (or Encircled Energy Fraction, EEF) and correspondingly the total flux of a source are also analytically characterized.

$$EEF(r) \equiv \int PSF(r)2\pi r dr = \frac{\pi r_c^2(1-W)}{1-\beta}((1+(\frac{r}{r_c})^2)^{1-\beta}-1) + 2\pi W\sigma^2(1-e^{-\frac{r^2}{2\sigma^2}})$$

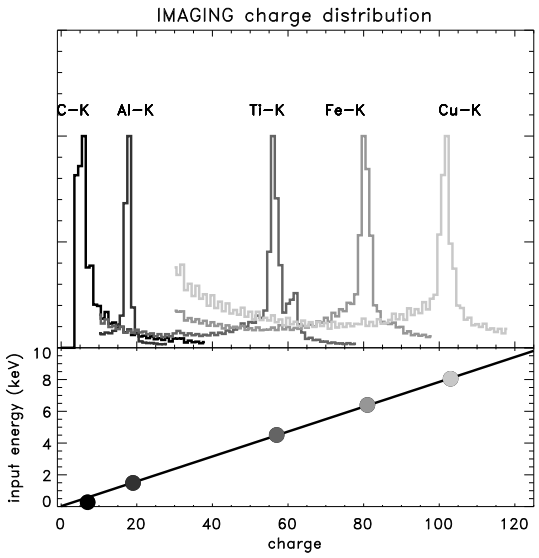

Figure 2. Imaging mode allows photon pileup to occur and no event reconstruction is performed. In this way most of the energy information of the original event is lost. But when all the charge is concentrated in one pixel the value of this pixel is well defined and it is a linear function of the energy (lower panel). In the upper panel the histograms of the pixel values from different images (arbitrarily normalized) at the five different calibration energies are plotted. In the lower panel the linearity of the relationship charge vs.energy is shown.

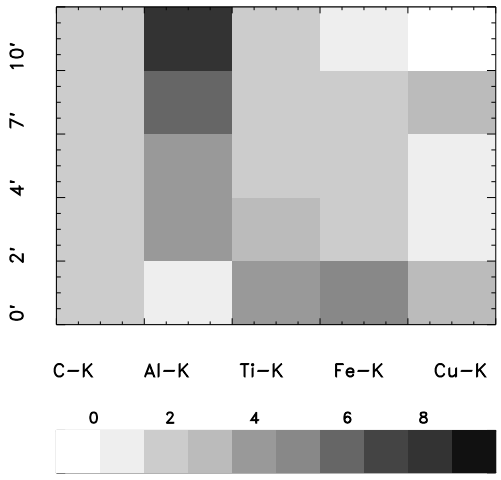

Figure 3. The numbers of reliable observations for our purpose binned in the Energy-Position plane. The bin referring to the Cu-K measurments at 10 arcmin off–axis angle is empty because the data do not match the selection criteria.

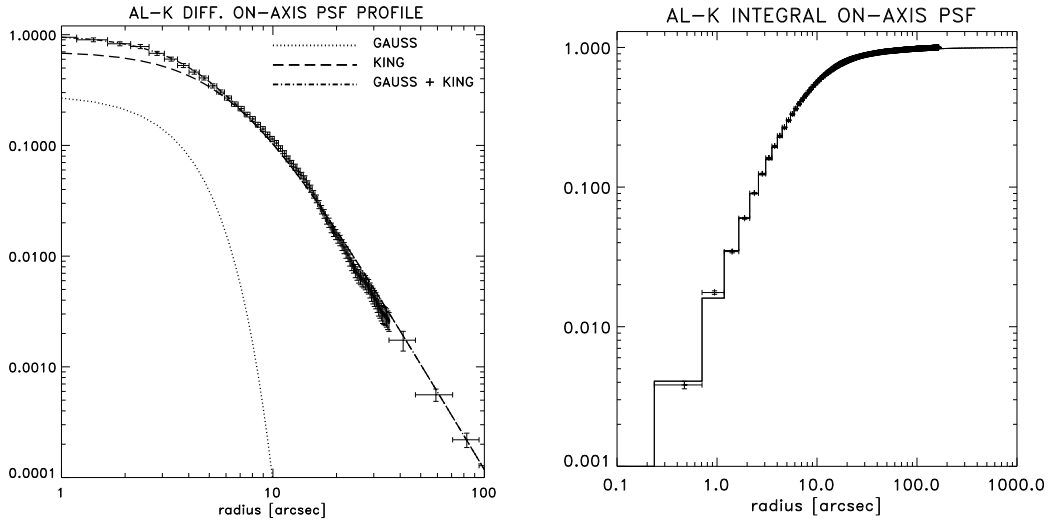

Figure 4. For each choice of energy and off–axis angle the PSF is well described by an analytical model which is the sum of a Gaussian plus a King function. Here as an example we plot the data and the model both for the differential and integral profile of the Al-K PSF (1.49 keV) on–axis.

$$EEF(\infty) = 2\pi W\sigma^2 + \pi r_c^2(1-W)/(\beta-1)$$

In Fig. 5 we plot the surface brightness profile for different energies on– and off–axis.

Table 2. The parameters of model (Eq. 1) which best describe the on-axis PSF at different energies.

	C-K	Al-K	Ti-K	Fe -K	Cu-K
W	0.34	0.29	0.25	0.19	0.15
σ[arcsec]	2.53	2.47	1.98	1.95	1.91
r_c[arcsec]	7.90	6.49	6.20	6.04	6.08
β	1.89	1.59	1.51	1.47	1.45

4. THE HALF ENERGY WIDTH

The Half Energy Width (HEW), defined as the diameter that contains 50% of the total flux, is a very useful parameter to test the quality of our optical system and to study the dependence of the PSF on the different energies and positions in the focal plane (Tab. 3). In the left panel of Fig. 6 the HEW values measured on–axis at the 5 calibration energies are reported: they range from $\sim$ 16 arcsec for C-K (0.28 keV) to $\sim$ 22 arcsec for Cu-K (8.05 keV). In the right panel of the same figure the HEW of the C-K line is plotted at different off–axis angles: the HEW on–axis is a local maximum and the HEW decreases for off–axis angles up to 7 arcmin. This

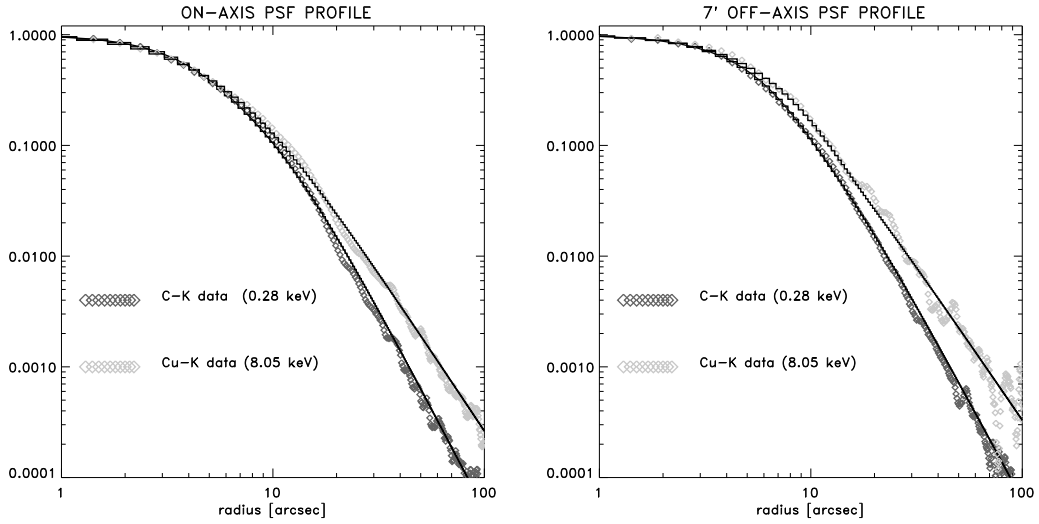

Figure 5. Examples of PSF profiles for two different energies in two different positions In both panels the diamonds are the data and the black solid line is the fit (Eq. 1).

is due to the fact that the CCD is intentionally offset slightly along the optical axis from the best on–axis focus: comparison with the HEWs expected from the ray tracing code indicate that the offset is about -2 mm. The consequence is that the PSF is slightly blurred on–axis and slightly better at $\sim$ 7 arcmin off–axis. Because of the particular operational procedures of the satellite, many XRT observations will be performed with the source not perfectly on–axis: the detector position represents a good trade-off between having a good spatial resolution and a larger field of view (this solution was also adopted by JET–X). In Tab. 3 we report also the HEWs measured during the calibration performed in July 2000 (with the CCD in focus) before the integration of the mirror module in the XRT tube. From the comparison with the actual values we measure the effect of the misalignment on the PSF. The actual measurements on–axis are somewhat worse, but still well under the scientific mission requirements. Moreover, from the right panel of Fig. 6 we can observe that the system is highly uniform on the central $\sim$8 arcmin region.

Table 3. In the table the HEW values on– and off–axis at different energies are reported. In the last column (FM3) the values measured for the mirror as a stand–alone unit during previous calibration tests are reported. All the values are in arcseconds.

	on–axis	off–axis(7 arcmin)	FM3 (on axis)	requirements
C-K	15.9 $\pm$0.3	14.9 $\pm$0.4	–	–
Al-K	17.6 $\pm$0.5	17.3 $\pm$0.7	14.0	20
Ti-K	19.4 $\pm$0.4	19.3 $\pm$0.2	17.3	–
Fe-K	20.7 $\pm$0.3	20.4 $\pm$0.3	–	–
Cu-K	22.2 $\pm$0.3	22.1 $\pm$0.5	20.3	30

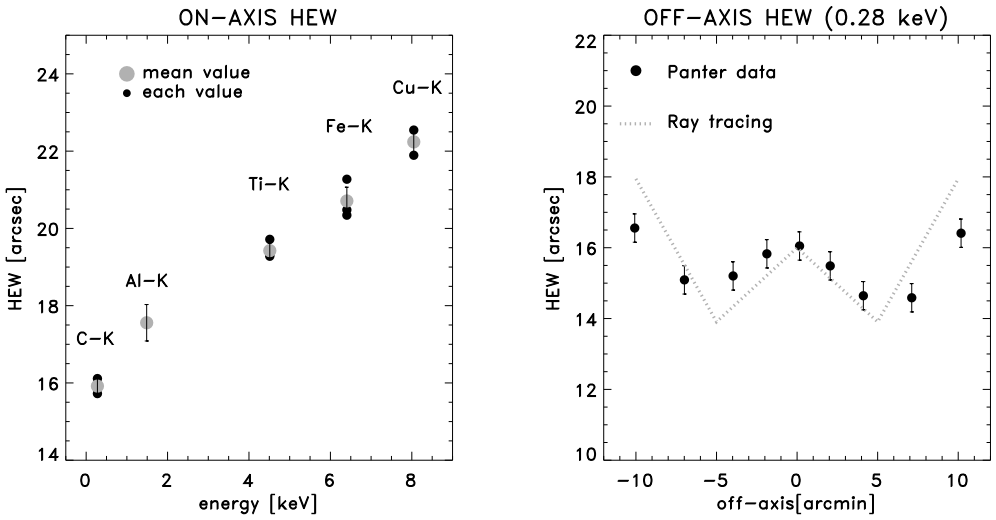

Figure 6. In the left panel the HEW on–axis measurements are plotted as a function of the energy. In the right panel the HEW of the C-K line is plotted for different off–axis positions. The negative values of the off–axis angle are conventionally assumed for the data taken in the left part of the detector. The laboratory data show a qualitative agreement with the results of the ray–tracing simulations for an out of focus position of -2 mm.

5. THE ANALYTICAL MODEL

The last step in our PSF analysis is the construction of an analytical model which describes the PSF as function of (E,θ). The main goal of building this model is the calculation of the PSF correction, which gives for a generic observed source the fraction of the flux contained in a given box. This is a fundamental ingredient in the photometric measurements and also in the construction of the Ancillary Response File (ARF) necessary for the spectroscopic analysis. As we can see from Tab. 2 the weight of the Gaussian W decreases with the energy. The core radius of the King function r_c increases with energy and the exponential β decreases allowing a steeper decrease for lower energies.

We performed a fit with the model (Eq. 1) on each element of the 5x5 grid of energy and off–axis values: for each of the 25 different sampling points in the energy–position plane we derived its four PSF parameter values (W, σ, r_c, β). In order to have an analytical model describing the PSF of sources with different spectra in different positions each parameter $par(E,\theta)$ has been fitted with a plane function of (E,θ) as illustrated in Fig.7:

$$par(E,\theta) = a + b \times \theta + c \times E + d \times E \times \theta \qquad (2)$$

The final aim of building the analytical model is to be able to give an accurate description of the PSF profile of a source with a generic spectrum in a generic position of the detector. In order to test if our model reaches this goal, we used the observations taken during the calibration campaign with a bremsstrahlung spectrum: they represent the most realistic test for our model because in the input spectrum all energies are sampled and it is

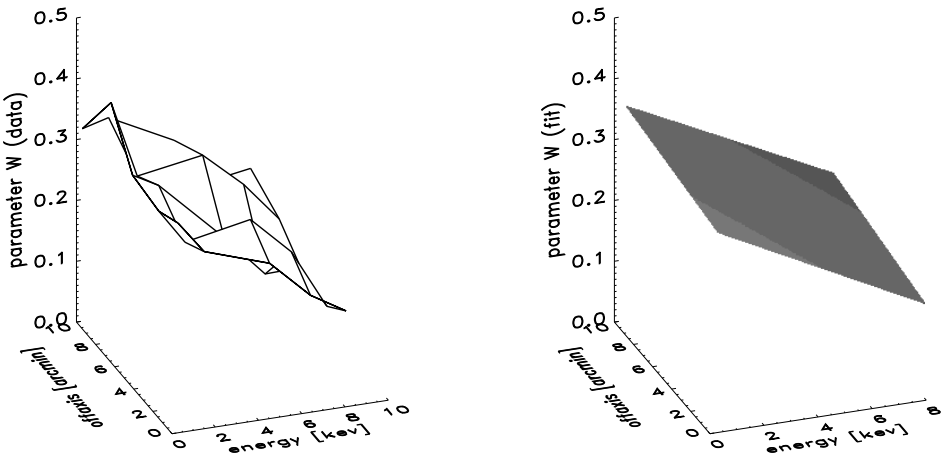

Figure 7. For each tested energy and position within the detector the PSF can be accurately described by the analytical model reported in (Eq. 1). This model has 4 free parameters and they are all functions of the energy and the off–axis angle. In order to provide an analytical model for a source with an arbitrary spectrum located at an arbitrary position on the detector, we fit each of the four parameters to a plane which is a function of energy and off-axis angle (Eq. 2). In this plot as an example we report the 25 different values (left panel) and the fit (right panel) of the parameter W, which gives the relative weight of the Gaussian function.

more similar to real astronomical sources. Using the model PSF=PSF(E,θ) for a grid of energy values we built a series of monochromatic images and summed them with the proper weights calculated from the normalized spectrum (for the energy grid we used a step of 100 eV ranging from 0.3 keV to 10.0 keV). The results of this procedure is reported in Fig.8. In the left panel the observed image is compared with the profile calculated with the model showing a very good agreement. More important, for our future work in the right panel we compare the integral profile of the test image with the model. As we can see from the residuals plot if we take a circle with the radius larger than 3 pixels ($\sim$ 7 arcsec) the model always describes the data with a precision better than 2%.

6. CONCLUSIONS

The PSF end-to-end calibration demonstrated that the XRT meets the mission requirements in terms of PSF and spatial resolution. Moreover through the detailed study of the PSF and the analytical model we demonstrated that we can calculate the PSF correction of the instrument with high accuracy for astronomical sources.

REFERENCES

1. D. Burrows, J. Hill, J. Nousek, A. Wells, A. Short, R. Ambrosi, G. Chincarini, and G.Tagliaferri, "The swift x-ray telescope (xrt)," *Proc. SPIE* **4851**, p. 1320B, 2003.

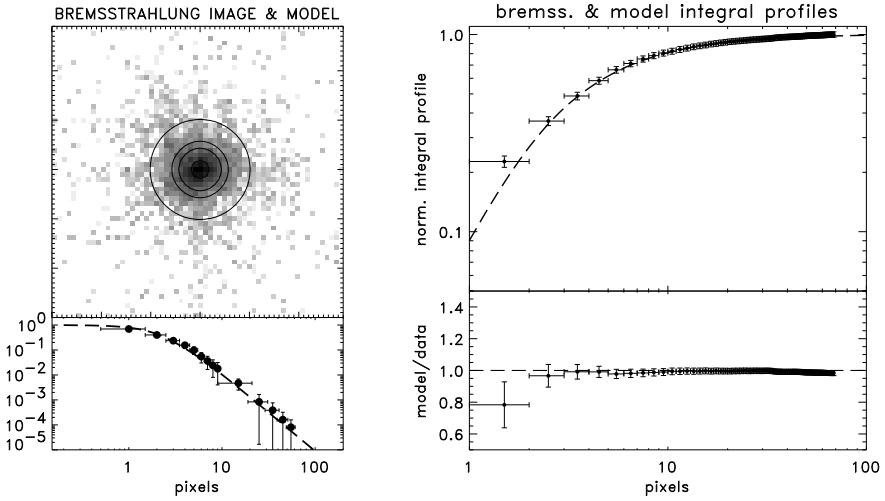

Figure 8. In the left panel the isophotes of the model are overplotted to the laboratory image. In the right panel we compare the integral profile of the test image with the model. As we can see from the residuals plot if we take a circle larger than 3 pixels the model describes the data with a precision better than 2%. (we stress again that here the model is not the best fit to the data but it is the reconstruction performed according to the procedures described in the text).

2. O. Citterio, S. Campana, P. Conconi, M.Ghigo, F. Mazzoleni, E. Poretti, G. Conti, G. Cusumano, B.Sacco, H.Braeuninger, W.Burkert, R. Egger, C. Castelli, and R. Willingale, "Characteristics of the flight model optics for the jet-x telescope onboard the spectrum x-γ satellite," *Proc. SPIE* **2805**, p. 56, 1996.
3. A. Wells, C. Castelli, M. Denby, D. Pullan, M. Sims, D. Watson, C. Withford, R. Willingale, C.J.Eyles, M.Cooke, W. Curtis, , H.Braeuninger, W.Burkert, R. Egger, O. Citterio, S. Campana, and G. Cusumano, "X-ray imaging performance of the flight model jet-x telescope," *Proc. SPIE* **3114**, p. 392, 1997.
4. D. Burrows, J. Hill, J. Nousek, A. Wells, A. Short, R. Willingale, O. Citterio, G. Chincarini, and G.Tagliaferri, "The swift x-ray telescope (xrt)," *Proc. SPIE* **4140**, p. 64, 2000.
5. O. Citterio, P. Conconi, M.Ghigo, R. Loi, F. Mazzoleni, E. Poretti, G. Conti, T. Mineo, B.Sacco, H.Braeuninger, and W.Burkert, "X-ray optics for the jet-x experiment aboard the spectrum-x satellite," *Proc. SPIE* **2279**, p. 480, 1994.